Turkish Journal of Electrical Engineering & Computer Sciences

http://journals.tubitak.gov.tr/elektrik/

Research Article

Turk J Elec Eng & Comp Sci
(2016) 24: 882 – 895

doi:10.3906/elk-1309-59

A generalized design method for multifunction converters used in a photovoltaic system

Trung Nhan NGUYEN[1,*], **An LUO**[2]
[1]Faculty of Electrical Engineering, Industrial University of Ho Chi Minh City, Ho Chi Minh, Vietnam
[2]School of Electrical and Information Engineering, Hunan University, Hunan, P.R. China

Received: 09.09.2013 • **Accepted/Published Online:** 20.01.2014 • **Final Version:** 23.03.2016

Abstract: In this paper, a general design method for multifunction converters using photovoltaic systems is proposed. With the proposed converter, the photovoltaic generator can provide flexibility, accuracy, and fast responses in both harmonic suppression and power injection modes in all cases of the grid-connected load. The controller for the proposed converter is designed based on the Lyapunov technique, along with the generalized algorithm for determining the global optimal values of the stability bounds. Therefore, the proposed converter can perform accurately and efficiently in the case of fixed system parameters as well as in the case of varying system parameters. Simulations and experimental results are presented to validate the accuracy and effectiveness of the proposed model and control strategy.

Key words: Photovoltaic system, power quality, multifunction controller, stability theory

1. Introduction

The world is currently faced with a continuous decrease in traditional fossil fuels as well as increasingly serious environmental pollution and warming due to the greenhouse effect. Consequently, the search for clean energy substitutes for traditional fossil fuels has attracted global attention. Renewable energy resources such as solar energy, wind energy, geothermal energy, and biofuel are appropriate and necessary alternatives. The introduction of renewable energy sources into the traditional power grid via distributed generation (DG) has led to the development of the microgrid concept. Many studies have aimed to efficiently exploit renewable energy resources. In these, solar energy seems more popularly exploited because of its advantages. The structural model of a photovoltaic (PV) system was presented in [1,2], and strategies for extracting power from PV systems at maximum power point operation were introduced in [3–5]. The PV system is an important module of a PV generator (PVG), acting as a primary energy source. For grid connection and power injection (POI) into the utility grid of PV systems, DC-DC converters and DC-AC inverters are used. Many researchers have recently proposed various strategies for connection and POI into the PVG utility grid [6,7]. In such works, the full controlling method used in the PVG generates maximum output power and it can be operated as a reactive power compensator. Using the controller presented in these works, the output reactive and active power of a PVG can be controlled simultaneously, similar to using a conventional synchronous generator in the power system.

The development of the PVG is essential to help solve the traditional energy crisis. However, the involvement of PVGs on the main grid, along with the increase of the nonlinear load, decreases the power

*Correspondence: nguyentrungnhan@hnu.edu.cn

quality (mainly due to harmonic currents), especially in the grid-connected case of the microgrid. The first solution to reduce the harmonic currents in the grid generated by the PVGs and nonlinear loads is to use active power filters (APFs). The APF model and control techniques have been studied, implemented, and effectively applied to the utility grid [8]. In [9–12], the authors presented a new hybrid APF model, which can be applied to medium- and high-voltage grids. Energy sources for the APF are usually taken from the main grid through a rectifier. Studies on the use of PV systems as a primary energy supply for APFs were analyzed and presented in [13,14].

The second solution is to improve the control quality of the DC/AC inverters. In [13,14], Wu et al. proposed a current controller based on amplitude-clamping and amplitude-scaling algorithms; this control method aims to prevent the output current from exceeding the switch rating and improve the flexibility of PVG in terms of changing operation modes. In this work, the active and reactive powers and distortions are controlled by complex control coefficients. Therefore, the stability of the control system depends on the control coefficients, and the system may be insecure. In [7,15–17], one solution for the injected power and harmonic compensation of the PVG system is to adopt a dual-level inverter. The advantages of this solution are its simplicity and the simultaneous realization of the POI into the utility grid and harmonic compensation. However, this is not an ideal solution, because it must be used through 2 IGBT bridges, which increases the costs of implementation, and the 2 inverters work as 2 separate converters. To overcome such problems, a flexible control method using the harmonic voltage signals for a voltage source inverter (VSI) was introduced in [18,19]. With this control method, the reference signal for the control system of DG is the harmonic voltage, and the DG can perform 2 functions simultaneously: injecting power into the utility grid and reducing the harmonic currents. However, the harmonic components of the voltage are very small compared to the currents. Therefore, the reference signal for the control system of the DG based on harmonic voltages will severely limit the sensitivity of the system, especially in the grid-connected mode of the microgrid.

Improvement of the effectiveness of the exploitation of PV systems has been implemented in previous works, as mentioned above. In practice, the total power-generating ability of PVGs is higher than the load power demand due to the abundance of solar radiation, and the power quality is not high, especially in the microgrid system. Furthermore, the operation of the system with high DG penetration does not guarantee spinning reserve and stability [20,21]. In this case, the best solution is to switch several DG systems from the POI to the harmonic suppression (HAS) mode. To do this, the controller of the DG must be flexible and intelligent. In [22], a multifunction converter (MFC) model for photovoltaic systems was proposed. In this model, a PVG can automatically or manually switch control between the 2 modes of working (POI mode or HAS mode) depending on the status of the utility grid, the weather conditions, and the requirements of the operator.

Existing methods only deal with the case of fixed system parameters (i.e. resistances, inductances, and capacitances). In real-world situations, however, system parameters may change over time and may not be determined accurately. As a result, performance quality and stability may not be obtained in real operation. To improve the quality, efficiency, and robustness of MFCs, this paper proposes a novel generalized method for designing the controller of MFCs.

Using the proposed method, the PVG controller can flexibly switch between HAS and POI modes, as achieved in [22], and can operate accurately and efficiently, even under varying system parameters. The controller of the proposed model is designed based on a combination of the Lyapunov technique and the

generalized algorithm for determining the optimal values of the stability bound. Simulations and experimental results are provided to validate the accuracy and effectiveness of the proposed model.

2. General system description

Figure 1 shows a single-line diagram of a three-phase PVG system connected to the power grid at the point of common coupling. It consists of PV arrays connected to a series with a DC-DC converter, called a PV-DC source block. The DC-DC converter acts as a solar energy extractor, ensuring operation at the maximum power point of the PV arrays. Next, the PV-DC source block is connected to a series with the VSI (note that in the dynamic analysis, the PV-DC source block can be considered as an equivalent capacitor C_e, as shown in Figure 1). In Figure 1, the inductor L_f and the capacitor C_f form a low-pass L-C filter that removes the high-frequency switching harmonics generated by the VSI of the PVG. The coupling inductor L_c (shown in Figure 1) acts as a connecting inductor; its main role is to reduce the current oscillation when there is a closed-open connection between the PVG and the main grid at the local bus. At the same local bus, a linear and a nonlinear load are also connected and unconnected through CB_{L1} and CB_{L2}. The amount of power actively injected into the main grid from the PVG is determined by the PV-DC source block output voltage and current. The MPPT control circuit is an important part of the PV-DC source; its objective is to set up the PV arrays output reference voltage corresponding to the PV maximum power [3–5]. The inputs of the MPPT controller are the output voltage and current of the PV-DC source block. The most important block in each PVG is the VSI, which acts as both the DC-AC converter and the MFC of the PVG in this work. The PCC- and DC-link bus voltages are sensed through the proper voltage-sensing circuitries, and the actual load and PVG currents are sensed using a current sensor. The sensed signals become the input signals of the control system. The details of the multipurpose control method for VSI based on the Lyapunov function are presented in the next section.

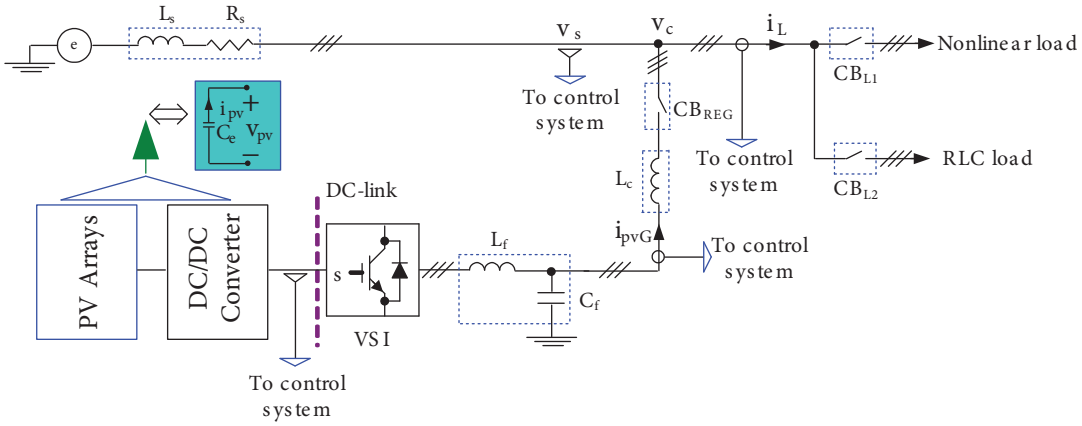

Figure 1. Single-line diagram of the proposed system.

3. Generalized design of the PVG control system based on the Lyapunov function

3.1. Mathematical model of the PVG in a d-q synchronous reference frame

As mentioned in [22], to simplify the calculation, capacitor C_f can be ignored. The resultant equivalent single-phase circuit of the PVG is shown in Figure 2, in which $R_{pv} \approx R_f + R_c$ and $L_{pv} \approx L_f + L_c$, where R_f and R_c are the internal resistances of inductances L_f and L_c, respectively. The state-space equations for the system shown in Figure 2 can be written in the d-q synchronous reference frame as follows (following the detailed analysis given in [22]):

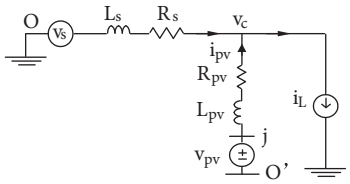

Figure 2. Equivalent single-phase circuit of the PVG system.

$$-v_{c\_d} - L_{pv}\dot{i}_{pv\_d} - R_{pv}i_{pv\_d} + \omega L_{pv}i_{pv\_q} + \delta_{n\_d}V_{DC-link} = 0, \tag{1}$$

$$-v_{c\_q} - L_{pv}\dot{i}_{pv\_q} - R_{pv}i_{pv\_q} - \omega L_{pv}i_{pv\_d} + \delta_{n\_q}V_{DC-link} = 0, \tag{2}$$

$$C_e\dot{V}_{DC-link} = \delta_{n\_d}i_{pv\_d} + \delta_{n\_q}i_{pv\_q}, \tag{3}$$

where the notation "$\bullet$" is the first-order derivative in time, and $\delta_{ns} = (u_s - \frac{1}{3}\sum_{j=a}^{c} u_{jo'})$ is defined as a switching state function, in which u_s is the switching function of the IGBT bridge (as presented in [22]). Eqs. (1)–(3) can be expressed using the matrices below.

$$\begin{bmatrix} \dot{i}_{pv\_d} \\ \dot{i}_{pv\_q} \\ \dot{V}_{DC-link} \end{bmatrix} = \begin{bmatrix} -\frac{R_{pv}}{L_{pv}} & \omega & \frac{\delta_{n\_d}}{L_{pv}} \\ -\omega & -\frac{R_{pv}}{L_{pv}} & \frac{\delta_{n\_q}}{L_{pv}} \\ \frac{\delta_{n\_d}}{C_e} & \frac{\delta_{n\_q}}{C_e} & 0 \end{bmatrix} \cdot \begin{bmatrix} i_{pv\_d} \\ i_{pv\_q} \\ V_{DC-link} \end{bmatrix} + \begin{bmatrix} -\frac{v_{c\_d}}{L_{pv}} \\ -\frac{v_{c\_q}}{L_{pv}} \\ 0 \end{bmatrix} \tag{4}$$

Let us choose

$$\begin{cases} x_1 = i_{pv\_d} - \tilde{i}_{pv-d} \\ x_2 = i_{pv\_q} - \tilde{i}_{pv-q} \\ x_3 = V_{DC\_link} - \tilde{V}_{DC-link} \end{cases}, \tag{5}$$

where x_1, x_2, and x_3 are the state variables of the PVG system; $\tilde{i}_{pv\_d}$ and $\tilde{i}_{pv\_q}$ are the reference currents calculated from the load; and $\tilde{V}_{DC-link}$ is the reference voltage at the DC-link bus. Substituting the aforementioned relations into Eq. (4), we have:

$$\begin{bmatrix} \dot{x}_1 \\ \dot{x}_2 \\ \dot{x}_3 \end{bmatrix} = \begin{bmatrix} \dot{\tilde{i}}_{pv\_d} \\ \dot{\tilde{i}}_{pv\_q} \\ \dot{\tilde{V}}_{DC-link} \end{bmatrix} + \begin{bmatrix} -\frac{R_{pv}}{L_{pv}} & \omega & 0 \\ -\omega & -\frac{R_{pv}}{L_{pv}} & 0 \\ \frac{\delta_{n\_d}}{C_e} & \frac{\delta_{n\_q}}{C_e} & 0 \end{bmatrix} \begin{bmatrix} i_{pv\_d} \\ i_{pv\_q} \\ V_{DC-link} \end{bmatrix}$$
$$+ \begin{bmatrix} 0 & 0 & \frac{\delta_{n\_d}}{L_{pv}} \\ 0 & 0 & \frac{\delta_{n\_q}}{L_{pv}} \\ \frac{\delta_{n\_d}}{C_e} & \frac{\delta_{n\_q}}{C_e} & 0 \end{bmatrix} \begin{bmatrix} 0 \\ 0 \\ V_{DC-link} \end{bmatrix} + \begin{bmatrix} -\frac{v_{c\_d}}{L_{pv}} \\ -\frac{v_{c\_q}}{L_{pv}} \\ 0 \end{bmatrix}. \tag{6}$$

Eq. (6) can be expressed in reduced form as follows:

$$\dot{x} = \dot{V} + Av + U + \zeta, \tag{7}$$

where $x = (x_1, x_2, x_3)^T$ and $v = (i_{pv\_d}, i_{pv\_q}, V_{DC-link})^T$. In Eq. (7), $U = (U_1, U_2, 0)^T$ and $\zeta = (\zeta_1, \zeta_2, 0)^T$ are the control signals and the disturbance inputs of the PVG control system, respectively. Please note that, in practice, the disturbances ζ in Eq. (7) consist of both the disturbances caused by voltage fluctuations and the unpredictable disturbances caused by the change in the system parameters, as mentioned in Section 1.

3.2. Preliminary design of the MFC control system based on the Lyapunov function

According to Lyapunov's stability theorem [23], a nonlinear system is globally and asymptotically stable if the Lyapunov candidate $V(x)$function satisfies $V(0) = 0$, $V(x) > 0 : x \neq 0$, $\dot{V}(x) < 0 : x \neq 0$, and $V(x) \to \infty$: $x \to \infty$for all x. In this paper, the control law for the PVG system is an error function defined to consist of 3 states based on the Lyapunov function method, as follows:

$$V = \frac{1}{2}(x_1^2 + x_2^2 + x_3^2), \tag{8}$$

where x_1, x_2, and x_3 are defined in Eq. (5). For system stability, the first derivative of $V(x)$ should be negative; to this end, without loss of generality, we can define the first derivative function as:

$$\dot{V} = \frac{\partial V(x)}{\partial x}\dot{x} = -x^T \lambda x, \tag{9}$$

where $\lambda = (\lambda_1, 0, 0; 0, \lambda_2, 0; 0, 0, \lambda_3)$ with λ_1, λ_2, and λ_3 as strictly positive quantities. By substituting Eqs. (6), (7), and (8) into (9), we have:

$$\begin{bmatrix} \lambda_1 x_1 \\ \lambda_2 x_2 \\ \lambda_3 x_3 \end{bmatrix} = \begin{bmatrix} \dot{\widetilde{i}}_{pv\_d} \\ \dot{\widetilde{i}}_{pv\_q} \\ \dot{\widetilde{V}}_{DC-link} \end{bmatrix} - \begin{bmatrix} -\frac{R_{pv}}{L_{pv}} & \omega & 0 \\ -\omega & -\frac{R_{pv}}{L_{pv}} & 0 \\ \frac{\delta_{n\_d}}{C_e} & \frac{\delta_{n\_q}}{C_e} & 0 \end{bmatrix} \begin{bmatrix} i_{pv\_d} \\ i_{pv\_q} \\ V_{DC-link} \end{bmatrix}$$
$$- \begin{bmatrix} 0 & 0 & \frac{\delta_{n\_d}}{L_{pv}} \\ 0 & 0 & \frac{\delta_{n\_q}}{L_{pv}} \\ \frac{\delta_{n\_d}}{C_e} & \frac{\delta_{n\_q}}{C_e} & 0 \end{bmatrix} \begin{bmatrix} 0 \\ 0 \\ V_{DC-link} \end{bmatrix} - \begin{bmatrix} -\xi_1 \\ -\zeta_2 \\ 0 \end{bmatrix}. \tag{10}$$

For a case with no disturbances (i.e. $\zeta = 0$), from Eq. (10), the switching state function of the control system can be expressed as:

$$\delta_{n\_d} = (\dot{i}_{pv\_d} + \frac{R_{pv}}{L_{pv}} i_{pv\_d} - \omega i_{pv\_q} - \lambda_1 x_1) \frac{L_{pv}}{V_{DC-link}}, \tag{11}$$

$$\delta_{n\_q} = (\dot{i}_{pv\_q} + \frac{R_{pv}}{L_{pv}} i_{pv\_d} + \omega i_{pv\_d} - \lambda_2 x_2) \frac{L_{pv}}{V_{DC-link}}, \tag{12}$$

where λ_1 and λ_2 are determined by the general stability condition of the Lyapunov function as follows:

$$\dot{V} = (x_1, x_2, x_3) \begin{bmatrix} -\lambda_1 x_1 - \zeta_1 \\ -\lambda_2 x_2 - \zeta_2 \\ -\lambda_3 x_3 - 0 \end{bmatrix} < 0. \tag{13}$$

Please note that the third condition of Eq. (13) is always satisfied; hence, from Eq. (13) we have the following general stability condition of the control system:

$$\begin{cases} \lambda_1 > \frac{|\zeta_1|_{\max}}{x_{10}} \\ \lambda_2 > \frac{|\zeta_2|_{\max}}{x_{20}} \end{cases}, \tag{14}$$

where x_{10} and x_{20} are the absolute error bounds of x_1 and x_2, respectively.

3.3. Impact analysis of unpredictable parameters on the stability condition

As mentioned in Section 1, the response of the control system is dependent on the actual values of the system parameters, such as resistances and inductances. Moreover, the change in the system parameters cannot be determined accurately. Without loss of generality, in this work we assume that the disturbance input of the control system of PVG (ζ) is a function of the system parameters. However, Eq. (4) shows that the dependence of the disturbances on the resistances is insignificant. Additionally, this equation also indicates that the voltage disturbances are small in comparison to the inductances and disturbances. Hence, to simplify the estimation in this paper, we focus only on the dependence of the disturbances on the inductances. Figure 3 shows the dependence of the values of $\xi_{\max}$ and λ on inductance L_e.

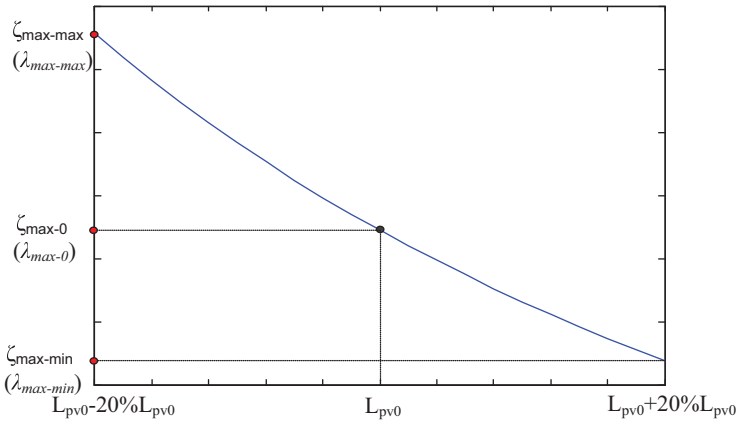

Figure 3. Relations between stability bounds and inductance Lpv.

3.4. Generalized design of the MFC control system

Figure 3 shows that the change in the disturbances (and the bound of the general stability condition) strongly depends on the change in the inductances. Therefore, the quality, stability, and target of the control systems will not be satisfied during operation unless the bounds of the general stability condition are determined accurately. In the proposed method, we assumed that the change in system parameters is limited to $\pm 20\%$ of the initial

values (i.e. $0.8\{L_{pv0}\} \leq \{L_{pvi}\} \leq 1.2\{L_{pv0}\}$). From Figure 3, the optimal values of the stability bounds under the condition of uncertain system parameters are as follows:

$$\begin{cases} \lambda_{1-optimal} > \frac{|\zeta_1|_{\max-\max}}{x_{10}} \\ \lambda_{2-optimal} > \frac{|\zeta_2|_{\max-\max}}{x_{20}} \end{cases} . \tag{15}$$

4. Implementation of the control system

A block diagram of the principle of the control system of the PVG proposed in this paper is shown in Figure 4. It consists of a phase-locked loop (PLL) module, transformer for transitioning from the three-phase coordinates to the dq0 frame, load current calculator, mode selector, use of the Lyapunov control technique to determine the control signal module, and pulse-width modulation generator. For the PLL module, to simplify the implementation and decrease the time delay, a PLL structure based on a second-order generalized integrator (SOGI-PLL) [24] is adopted in this work. The load and PVG output currents i_L and i_{pv} are converted from the three-phase coordinates to the dq0 coordinates. The fundamental frequency and harmonic components of the load current are determined with the load current calculator. Accurate estimation and measurement of the fundamental and harmonic currents is important. If the power frequency of the signal is steady and near the nominal value, the discrete Fourier transform (DFT) can be used to achieve good estimation performance. However, there are considerable power frequency variations in an isolated system, such as a microgrid working in stand-alone mode. These variations may introduce substantial phase errors in the estimates if the DFT is adopted. To address this problem and easily realize a digital signal processor (DSP) for real-time implementation, the sliding discrete Fourier transform (SDFT) [25] is used in the calculation of the load current. The inside of the circuit diagram of the load current's calculation block, using the SDFT technique, is expressed in detail in [22]. The output of this block yields the load fundamental current i_{LF_dq}, the load harmonic current i_{LH_dq}, and the total harmonic distortion (THD) of the load current. The next block is the mode selector, which allows the user to select the operation modes. When the manual modes are used, the PVG is only operating in a single mode (HAS or POI) during operation. In contrast, in the automatic mode, the MFC will automatically change to operating mode according to the input signals, such as the THD of the load current, the balance between power generation and power demand in the main grid, and weather conditions. The threshold of the input control signals can be changed using control programs. The MFC in this paper is designed based on the Lyapunov control technique. This is the most important module and the center of the control system used in the PVG. The input signals of the MFC consist of (as shown in Figure 4) the output of the mode selector (1, 2, or 3), outputs of the current calculator (i_{LF_dq}, i_{LH_dq}, THD), DC-link bus voltage and its reference value, VSI output current (i_{pv-dq}), and PCC voltage. The main role of this block is to create a global switching function through Eqs. (11) and (12) to the PWM generator module in all operating situations of the PVG.

5. Simulation and experimental results

5.1. Simulation results

The proposed model and the flexible control strategies based on Lyapunov's stability theory are verified through simulation in the MATLAB/Simulink environment. The main purpose of the simulation is to test the effectiveness and accuracy of the control strategy used in PVG in various operation modes. In this simulation,

the main frequency of the power grid is 50 Hz, and the harmonic current sources are generated by the half-wave three-phase diode rectifier. Moreover, the power grid voltage in this simulation is 380 V (phase-phase), and the control signal of the IGBTs is generated using a pulse-width modulation generator, such that the amplitude and frequency of the carrier wave are ±100 V and 10 kHz, respectively. The detailed control parameters used in the simulations are given in the Table below and could be changed through keyboard input.

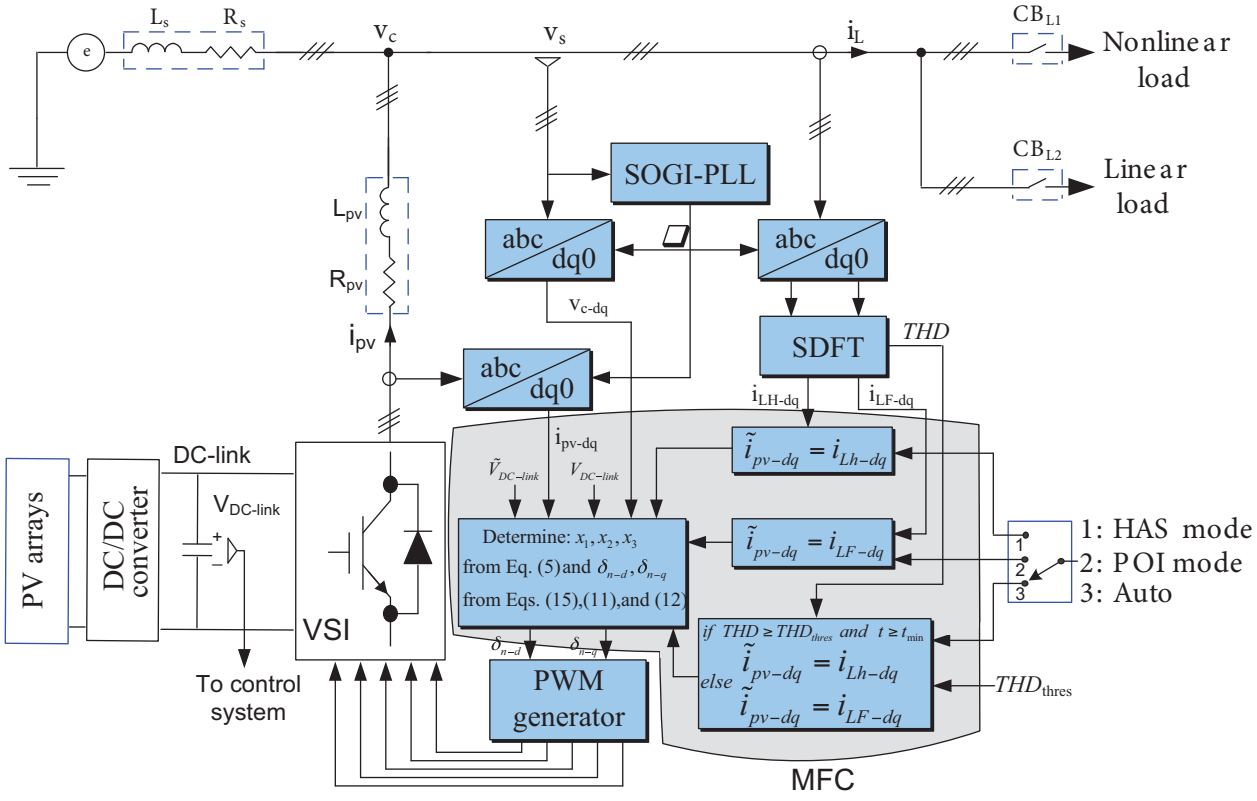

Figure 4. Block diagram of the control system used in PVG.

Table. Parameters used in the simulations.

AC grid line-line voltage	V_s = 380 V (rms)
AC grid frequency	f = 50 Hz
Source impedance	L_s = 0.2 mH, R_s = 0.08 Ω
Low-pass L-C filter	R_f = 0.1 Ω, L_f = 1 mH, C_f = 0.1 μF
Coupling inductor	R_c = 0.1 Ω, L_c = 1 mH
Switching frequency	f_s = 10000 Hz

As shown in this figure, the PVG always operated as a power generator in this mode, even if the THD of the load current significantly increased. Moreover, in this case, the power injected into the main grid is always equal to the maximum power extracted from the photovoltaic system, even if the power load changes (at t = 0.1 s and through 2 circuit breakers, CB_{L1} and CB_{L2}). In contrast to the POI mode, in the HAS mode the PVG always operated as an active power filter. Figure 6 shows the simulation results in this mode, indicating that the grid current has almost eliminated the harmonic elements, whereas the power injected into the main grid from the PVG is almost zero. Note that if the THD of the load current is negligible, PVG-connected grid presence does not affect the power quality of the main grid in this mode (as shown in Figure 6 before t = 0.1 s).

To verify their effectiveness and accuracy under all conditions, the simulations are realized in 3 modes under different load currents. Figure 5 illustrates the simulation results of the PVG system in the POI mode. PCC voltage, load current (i_{La}), grid current (i_{sa}), and PVG current (i_{pva}) are included in phase (a).

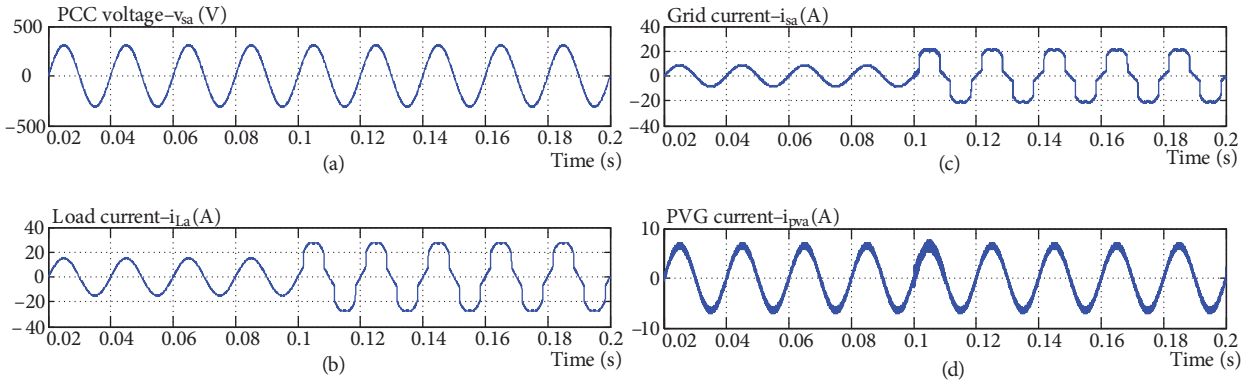

Figure 5. Simulation results in POI mode: (a) PCC voltage, (b) load current, (c) grid current, and (d) PVG current.

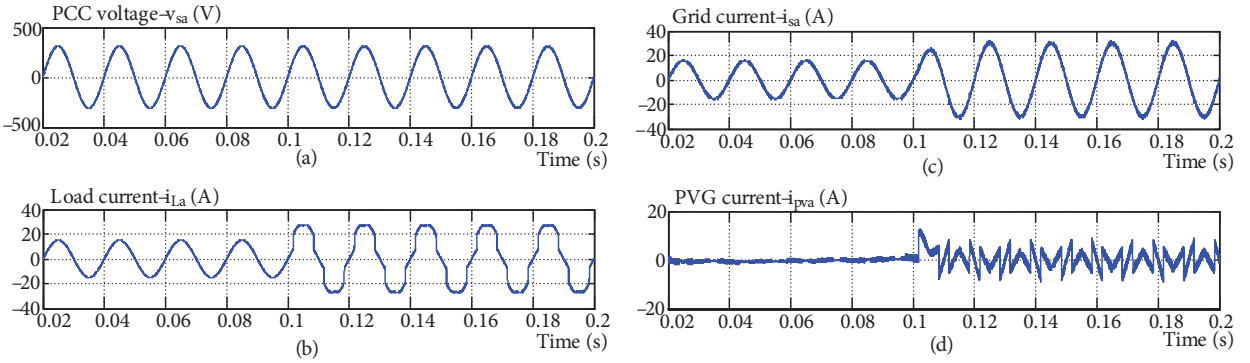

Figure 6. Simulation results in HAS mode: (a) PCC voltage, (b) load current, (c) grid current, and (d) PVG current.

We now consider a PVG operated in AUTO mode under various power loads. The power loads vary among 3 levels: a linear load (with the THD of the load current being less than the threshold THD, and the load power being larger than the maximum power of the PV arrays), a nonlinear load (with the THD of the load current exceeding the threshold THD), and another linear load (with the load power being less than the maximum power of the PV arrays). At first, a linear load similar to the prior simulations is connected to the PCC. At t = 0.1 s, a nonlinear load is connected to the PCC. This process is continued until t = 0.2 s, at which time the prior loads (linear and nonlinear) are removed and another linear load (in which the power capacity is less than the maximum power extracted from the PV arrays) is connected. The simulation results are shown in Figure 7, revealing that the proposed model can provide flexibility, accuracy, and fast responses.

In Figure 7, at t = 0.1 s, the proposed PVG automatically changes from POI to HAS mode (because THD is larger than THD_{thres}), and the responses of the power and current are the same as in prior simulations. At t = 0.2 s, the PVG automatically reverts to POI mode. In addition, after t = 0.2 s, all the load power is provided by the PVG, and the remaining PVG power is injected into the main grid (because the maximum power extracted from the PV arrays is larger than in the grid-connected load in this case). This leads to the grid current phrase being antiphase with the PCC voltage, as shown in Figure 7. A more detailed observation of the power response of the proposed model is shown in Figure 8.

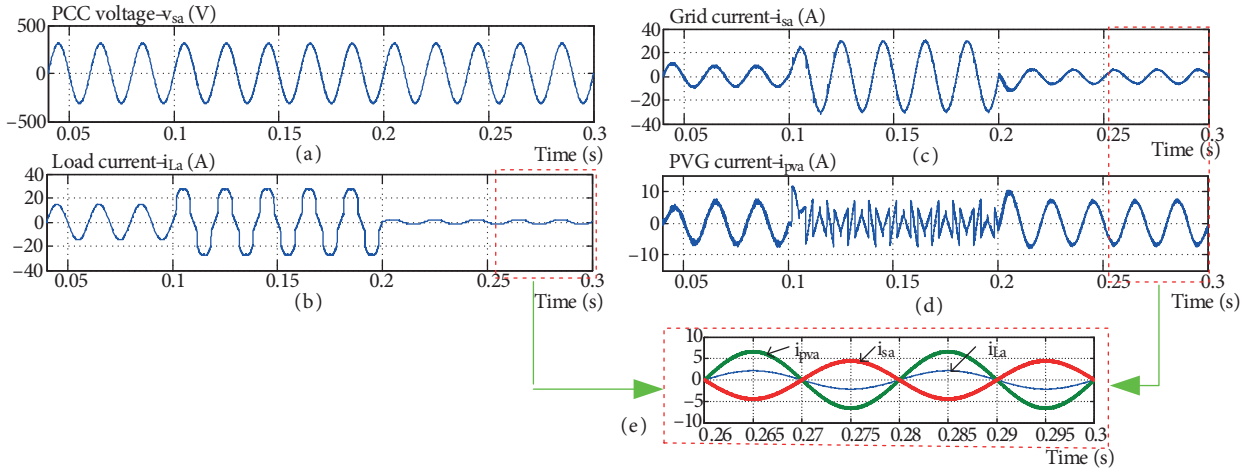

Figure 7. Simulation results in AUTO mode: (a) PCC voltage, (b) load current, (c) grid current, (d) PVG current, and (e) enlarged view.

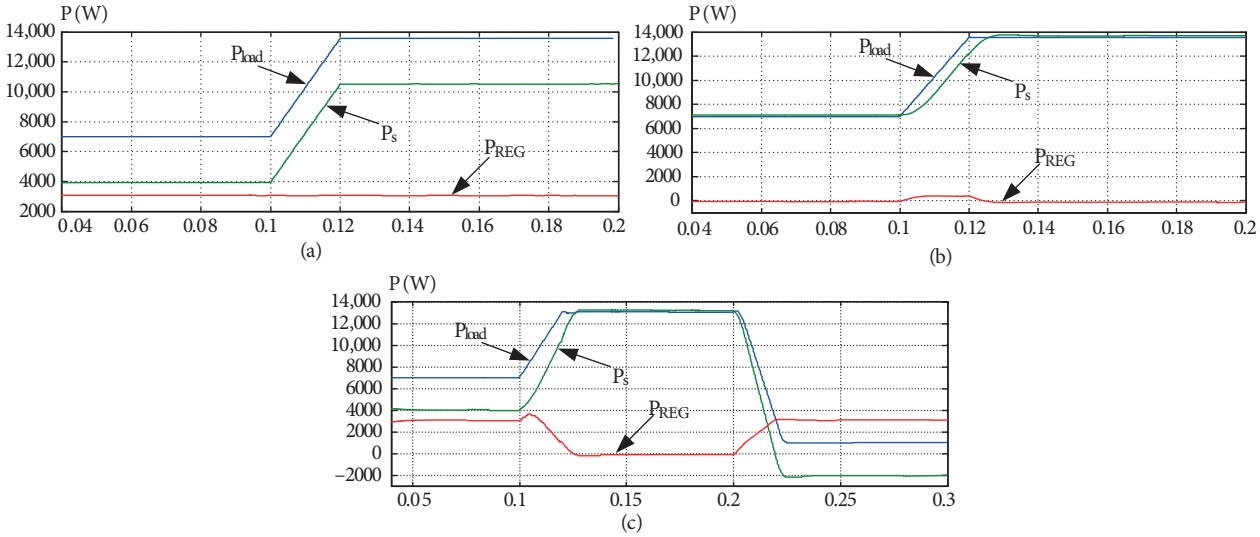

Figure 8. Power responses: (a) POI mode, (b) HAS mode, and (c) AUTO mode.

In brief, the simulation results show that the proposed PVG model can provide flexibility, accuracy, and fast responses in all cases of the grid-connected load. In the HAS mode, the harmonic elements of the grid current have been virtually eliminated, while in the POI mode, the power injected into the main grid (including grid-connected loads) from the PVG is always equal to the maximum power extracted from the PV arrays. This helps exploit renewable energies more effectively.

We now consider a variable system parameter case. In this simulation, we assumed that the change of system parameters is limited to $\pm 10\%$ of the initial value. The responses of the currents under variations of system parameters are shown in Figure 9. Figure 9 shows that when the method of [22] is used, the error of the control system significantly increases. However, if the proposed method is used, the error of the control system is just a negligible change, and the quality of the PVG system is still achievable.

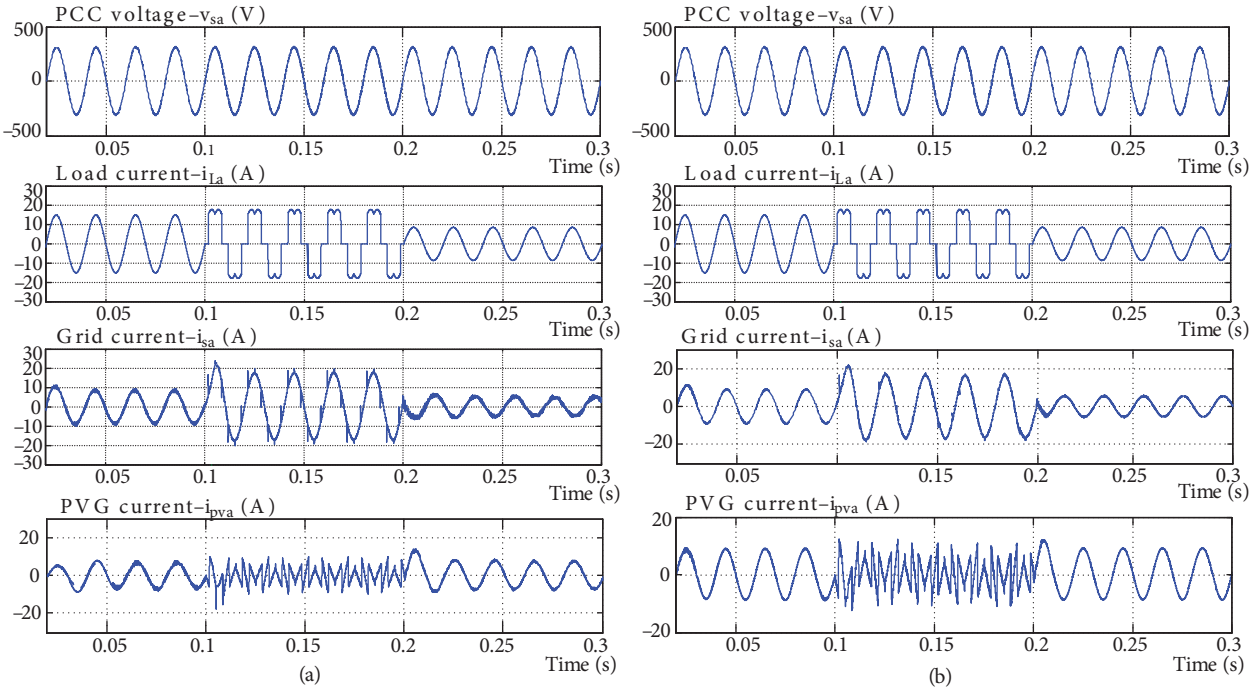

Figure 9. Currents responses under variations of system parameters: (a) method presented in [22], (b) proposed method.

5.2. Experimental results

To confirm the effectiveness of the PVG with the proposed topology and control strategy, experiments were conducted employing a laboratory test system on a 60-kVA setup. A TI TMS320F2812 DSP is used to implement the control methods based on Eqs. (5), (11), and (12) with a sampling frequency f =10 kHz. The control parameters are the same as those in the simulations and can be changed through keyboard input. The renewable energy resources in these experiments are the PV arrays, with a total peak power of 5 kW. In these experiments, the nonlinear load is taken to be a half-wave three-phase rectifier terminated to a resistive assembly, and the linear load is a resistive load. The experimental results for the POI mode are shown in Figure 10. As shown in this figure, the PVG always operated as a power generator in this mode, even when the THD of the load current increased significantly. Moreover, in this case, the power injected into the main grid is always equal to the maximum power extracted from the PV arrays, even if the power load changes. Figure 11 shows the experimental results for the HAS mode.

In this experiment, the load current is the same as in the prior experiment. Figure 11 shows that, in this case, the PVG always operated as an active power filter, and the grid current almost eliminated the harmonic elements. Furthermore, the power injected from PVG into the main grid is almost zero. Figure 12 shows the experimental results in AUTO mode. In this experiment, the load current is changed from a linear load to a nonlinear load. When the load current is linear (the THD of the load current is less than the threshold THD), the PVG operates in POI mode. It automatically changes to HAS mode if the THD of the load current is larger than the threshold THD. From these figures, it can be seen that the proposed PVG model operates correctly in all modes. Additionally, the proposed controller has good steady-state and dynamic response characteristics regardless of whether the load is changed or not.

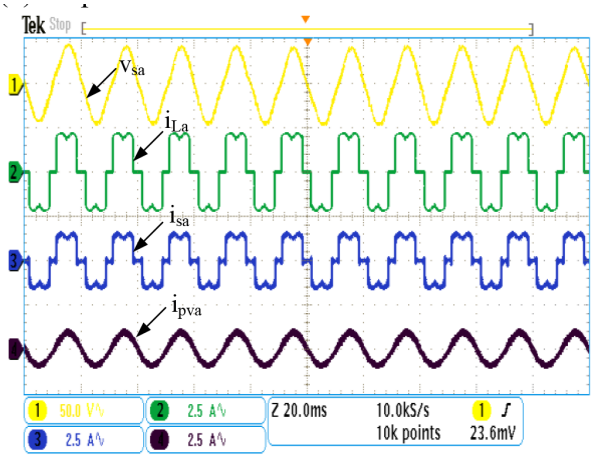

Figure 10. Experimental results in POI mode.

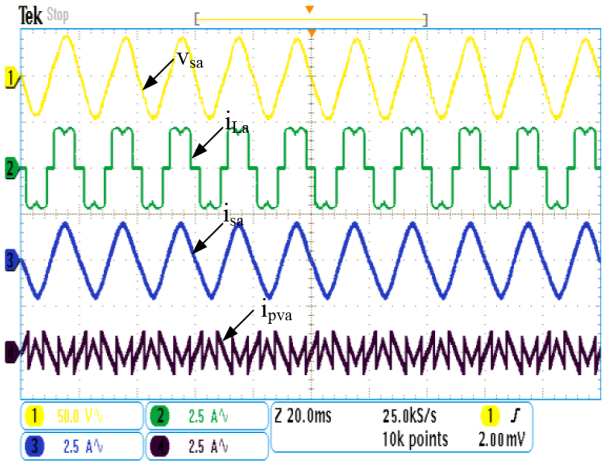

Figure 11. Experimental results in HAS mode.

Similar to the simulations, in order to demonstrate the effectiveness and correctness of the proposed method, the experiments were performed for various system parameters. The experimental results for this case are shown in Figure 13. They yet again confirm that the system performance is sensitive to the system parameters and only can achieve good performance under various system parameters if the values of λ_1 and λ_2 are exactly determined as in Eq. (15). Therefore, the exact determination of stability bounds of the MFC, especially in the case of the change of system parameters, is important and should be done carefully.

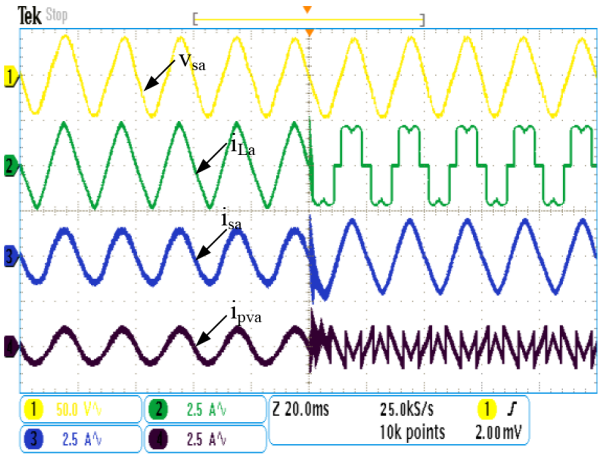

Figure 12. Experimental result in AUTO mode.

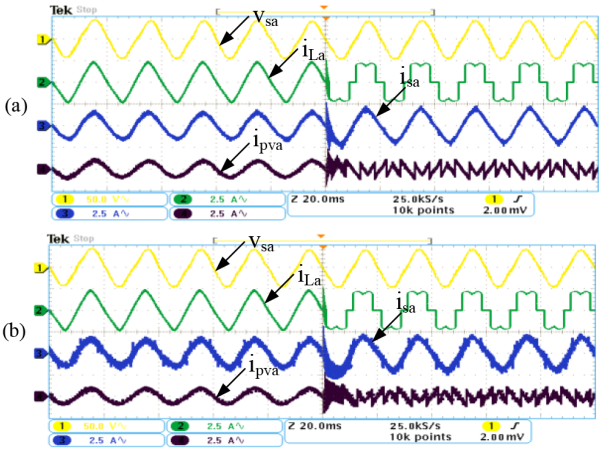

Figure 13. Experimental results in AUTO mode under various system parameters: (a) proposed method, (b) method presented in [22].

6. Conclusion

In this paper, a generalized design method for MFCs used in photovoltaic-based inverters is proposed. Using the proposed model, a photovoltaic generator can provide flexible, accurate, and fast responses for both POI and HAS modes. The influence of the system parameters on the quality of the control system in PVG was also analyzed in detail. It was shown that the robustness and stability of the control system are highly dependent

on the system parameters. Moreover, the system parameters cannot be accurately determined, because their values depend on elements such as the environment temperature, operating time, and equipment quality. The controller proposed in this paper is designed based on the Lyapunov technique and the generalized algorithm for determining the global optimal values of the stability bounds. It guarantees that the proposed converter will perform accurately and efficiently both in the case of fixed system parameters and in that of varying system parameters. The other advantage of the proposed controller is its fast dynamic response and small steady-state error in tracking the current signal. Simulation and experimental results have been obtained to demonstrate the robustness and effectiveness of the proposed model and control strategy. The experimental results confirm that the system performance is sensitive to the system parameters and can only achieve good performance under various system parameters if the values of the stability bounds are exactly determined. Therefore, exact determination of the stability bounds of the MFC, especially in the case of change in system parameters, is important and should be done carefully.

The proposed model and control strategy are a powerful approach to improving the power quality and optimal operation in a power grid, including a microgrid system.

Acknowledgments

This work was supported in part by the National Natural Science Foundation of China (Grant No. 60774043), National Basic Research Program of China (Program 863, Grant No. 2009CB219706), and National Natural Science Youth Foundation (Grant No. 50907017).

References

[1] Bae S, Kwasinski A. Dynamic modeling and operation strategy for a microgrid with wind and photovoltaic resources. IEEE T Smart Grid 2012; 3: 1867–1876.

[2] Petrone G, Ramos-Paja C. Modeling of photovoltaic fields in mismatched conditions for energy yield evaluations. Electr Pow Syst Res 2011; 81: 1003–1013.

[3] Ahmed NA, Miyatake M. A novel maximum power point tracking for photovoltaic applications under partially shaded insolation conditions. Electr Pow Syst Res 2008; 78: 777–784.

[4] Hussein KH, Muta I, Hoshino T, Osakada M. Maximum photovoltaic power tracking: an algorithm for rapidly changing atmospheric conditions. IEE P-Gener Transm D 1995; 142: 59–64.

[5] Valderrama-Blavi H, Bosque JM, Guinjoan F, Marroyo F, Martinez-Salamero L. Power adaptor device for domestic DC microgrids based on commercial MPPT inverters. IEEE T Ind Electron 2013; 60: 1191–1203.

[6] Wu LB, Zhao ZM, Liu JZ. A single-stage three-phase grid-connected photovoltaic system with modified MPPT method and reactive power compensation. IEEE T Energy Conver 2007; 22: 881–886.

[7] Miñambres-Marcos V, Romero-Cadaval E, Guerrero-Martínez MA, Milanés-Montero MI. Cooperative operation of inverters for grid-connected photovoltaic generation systems. Electr Pow Syst Res 2013; 96: 47–55.

[8] Singh B, Al-Haddad K, Chandra A. A review of active filters for power quality improvement. IEEE T Ind Electron 1999; 46: 960–971.

[9] Luo A, Tang C, Shuai ZK, Zhao W, Rong F, Zhou K. A novel three-phase hybrid active power filter with a series resonance circuit tuned at the fundamental frequency. IEEE T Ind Electron 2009; 56: 2431–2440.

[10] Chau M, Luo A, Ma F, Shuai ZK, Nguyen TN, Wang W. Online control method with time-delay compensation for hybrid active power filter with injection circuit. IET Power Electrons 2012; 5: 1472–1482.

[11] Shuai ZK, Luo A, Zhu WJ, Fan RX, Zhou K. Study on a novel hybrid active power filter applied to a high-voltage grid. IEEE T Power Deliver 2009; 24: 2344–2352.

[12] Luo A, Peng SJ, Wu CP, Wu JB, Shuai ZK. Power electronic hybrid system for load balancing compensation and frequency-selective harmonic suppression. IEEE T Ind Electron 2012; 59: 723–732.

[13] Wu TF, Nien HS, Shen CL, Chen TM. A single-phase inverter system for PV power injection and active power filtering with nonlinear inductor consideration. IEEE T Ind Appl 2005; 41: 1075–1083.

[14] Wu TF, Nien HS, Hsieh HM, Shen CL. PV Power injection and active power filtering with amplitude-clamping and amplitude-scaling algorithms. IEEE T Ind Appl 2007; 43: 731–741.

[15] Li YW, Vilathgamuwa DM, Loh PC. Microgrid power quality enhancement using a three-phase four-wire grid-interfacing compensator. IEEE T Ind Appl 2005; 41: 1707–1719.

[16] Li J, Zhuo F, Wang XW, Wang L, Ni S. A grid-connected PV system with power quality improvement based on boost + dual-level four-leg inverter. In: IEEE 2009 Power Electronics and Motor Control Conference; 17–20 May 2009; Wuhan, China. New York, NY, USA: IEEE. pp. 436–440.

[17] Li J, Zhuo F, Liu JJ, Wang XW, Wen B, Wang L, Ni S. Study on unified control of grid-connected generation and harmonic compensation in dual-stage high-capacity PV system. In: IEEE 2009 Energy Conversion Congress and Exposition; 20–24 September 2009; San Jose, CA, USA. New York, NY, USA: IEEE. pp. 3336–3342.

[18] Gajanayake CJ, Vilathgamuwa DM, Loh PC, Teodorescu R, Blaabjerg F. Z-source-inverter-based flexible distributed generation system solution for grid power quality improvement. IEEE T Energy Conver 2009; 24: 695–704.

[19] He JW, Li YW, Munir MS. A flexible harmonic control approach through voltage-controlled DG–grid interfacing converters. IEEE T Ind Electron 2012; 59: 444–455.

[20] Safigianni AS, Koutroumpezis GN, Poulios VC. Mixed distributed generation technologies in a medium voltage network. Electr Pow Syst Res 2013; 96: 75–80.

[21] Pandi VR, Zeineldin HH, Weidong Xiao, Zobaa AF. Optimal penetration levels for inverter-based distributed generation considering harmonic limits. Electr Pow Syst Res 2013; 97: 68–75.

[22] Nguyen TN, Luo A. Multifunction converter based on Lyapunov function used in a photovoltaic system. Turk J Electr Eng Co 2014; 22: 893–908.

[23] Haddad WH, Chellaboina VS. Nonlinear Dynamical Systems and Control: A Lyapunov-Based Approach. Princeton, NJ, USA: Princeton University Press, 2008.

[24] Ciobotaru M, Teodorescu R, Blaabjerg F. A new single-phase PLL structure based on second order generalized integrator. In: IEEE Power Electronics Specialists Conference; 18–22 June 2006; Jeju, South Korea. New York, NY, USA: IEEE. pp. 1–6.

[25] Jacobsen E, Lyons R. The sliding DFT. IEEE Signal Proc Mag 2003; 20: 74–80.